Detections of two GRBs above 100 GeV by MAGIC and HESS

A very-high-energy component deep in the γ-ray burst afterglow
H.E.S.S. collaboration; *Nature 575*, 464-467 (2019)
https://www.nature.com/articles/s41586-019-1743-9
also available on arXiv: https://arxiv.org/abs/1911.08961

Teraelectronvolt emission from the γ-ray burst GRB 190114C
MAGIC collaboration; *Nature* 575, 455-458 (2019)
https://www.nature.com/articles/s41586-019-1750-x

Observation of inverse Compton emission from a long γ-ray burst
MAGIC collaboration; *Nature* 575, 459-463 (2019)
https://www.nature.com/articles/s41586-019-1754-6

Detections of two GRBs above 100 GeV by MAGIC and HESS

A very-high-energy component deep in the γ-ray burst afterglo
H.E.S.S. collaboration; *Nature 575*, 464-467 (2019)
https://www.nature.com/articles/s41586-019-1743-9
also available on arXiv: https://arxiv.org/abs/1911.08961

GRB 180720B

Teraelectronvolt emission from the γ-ray burst GRB 190114C
MAGIC collaboration; *Nature* 575, 455-458 (2019)
https://www.nature.com/articles/s41586-019-1750-x

GRB 190114C

Observation of inverse Compton emission from a long γ-ray bu
MAGIC collaboration; *Nature* 575, 459-463 (2019)
https://www.nature.com/articles/s41586-019-1754-6

GRB 190114C
Multi-λ follow-up

Basic facts:

- **GRB180720B:**
  - Redshift: z = 0.653 – Duration: T_{90} ~ 50 s (**long cosmological GRB**)
  - E_{iso} = 6.0 ± 0.1 10^{53} erg (50-300 keV)
  - Detected by GBM & BAT (trigger), LAT (during 12 min), XRT and many others
  - Afterglow detectable for ~ 30 days
  - **HESS: VHE detection 10 hours after the burst: afterglow phase**
  - Fermi/GRM: 7th brightest GRB ; Swift/XRT: 2nd brightest afterglow

- **GRB190114C:**
  - Redshift: z = 0.4245 – Duration: T_{90} ~ 116 s (GBM) – 362 s (BAT) (**long cosmological GRB**)
  - E_{iso} = 3 10^{53} erg (1-10000 keV)
  - Detected by BAT & GBM (trigger), INTEGRAL, LAT (during 12 min), AGILE, XRT and many other
  - **MAGIC: VHE detection (0.2-1 TeV) 1 minute after the burst at 50 sigmas during the first 20 min – observed for 40 min**

    at 80 s: 3 10^{49} erg/s (0.3-1 TeV) = most luminous source known at VHE

    Total observation: 4 10^{51} erg (0.3-1 TeV)

GRB 180720B (HESS)

GRB180720B: HESS image

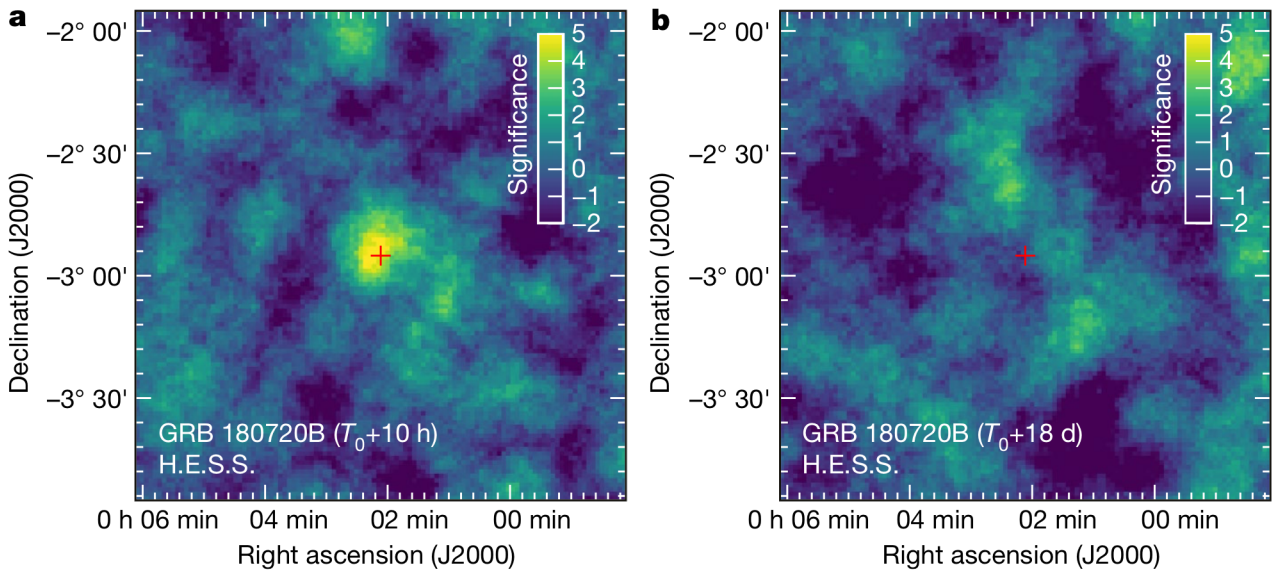

Fig. 2 | Very-high-energy γ-ray image of GRB 180720B. Significance map of GRB 180720B field, as observed by H.E.S.S. **a**, Observation made at T_0 + 10.1 h for 2 h. **b**, The same region of the sky, as observed during consecutive nights between T_0 + 18.4 d and T_0 + 24.4 d. The red cross indicates the position reported by the optical telescope ISON-Castelgrande[12].

- Obs: T_0+10,1h – 2 hours
- 119 gamma-ray events – statistical significance = 5.3 sigmas
- Point-like source model
- Re-observation several days later: no detection

A very-high-energy component deep in the γ-ray burst afterglow, H.E.S.S. collaboration; *Nature 575*, 464-467 (2019)

GRB180720B: light-curve

$\alpha_{XRT} \sim \alpha_{opt} \sim -1.3/-1.2$
$\alpha_{LAT} \sim -1.8$; $\gamma_{LAT} \sim -2.1$

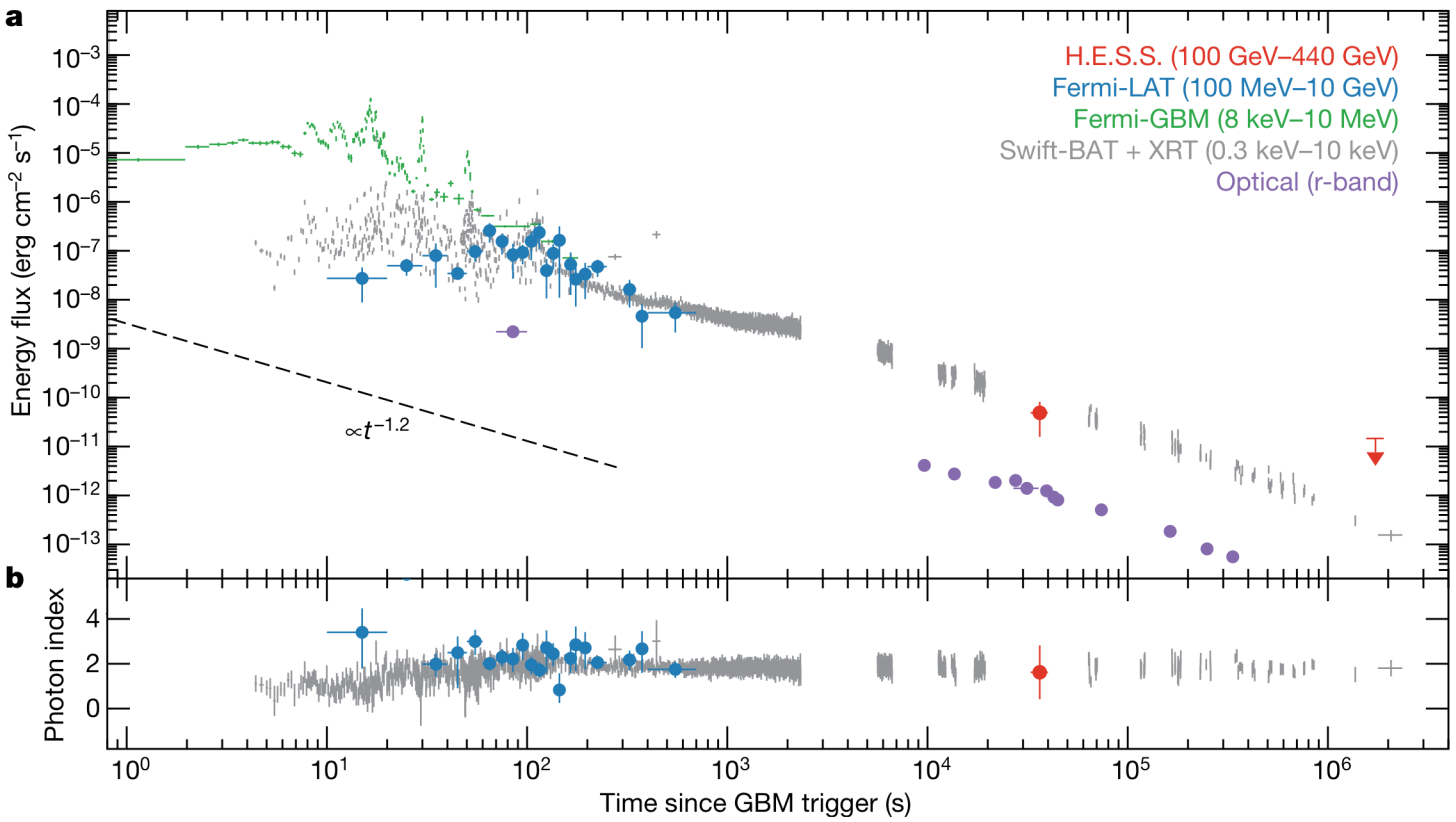

Fig. 1 | Multi-wavelength light curve of GRB 180720B. a, Energy-flux light curve detected by Fermi-GBM (band fit; green), Fermi-LAT (power law; blue), H.E.S.S. (power-law intrinsic; red) and the optical r-band (purple). The Swift-BAT spectra (15 keV–150 keV) are extrapolated to the XRT band (0.3–10 keV) to produce a combined light curve (grey) and an upper limit (95% confidence level) for the second H.E.S.S. observation window (power-law intrinsic, red arrow). The black dashed line indicates a temporal decay with $\alpha = -1.2$. **b**, Photon index of the Fermi-LAT, Swift and H.E.S.S. spectra. Error bars correspond to 1σ.

A very-high-energy component deep in the γ-ray burst afterglow, H.E.S.S. collaboration; *Nature 575*, 464-467 (2019)

GRB180720B: VHE spectrum

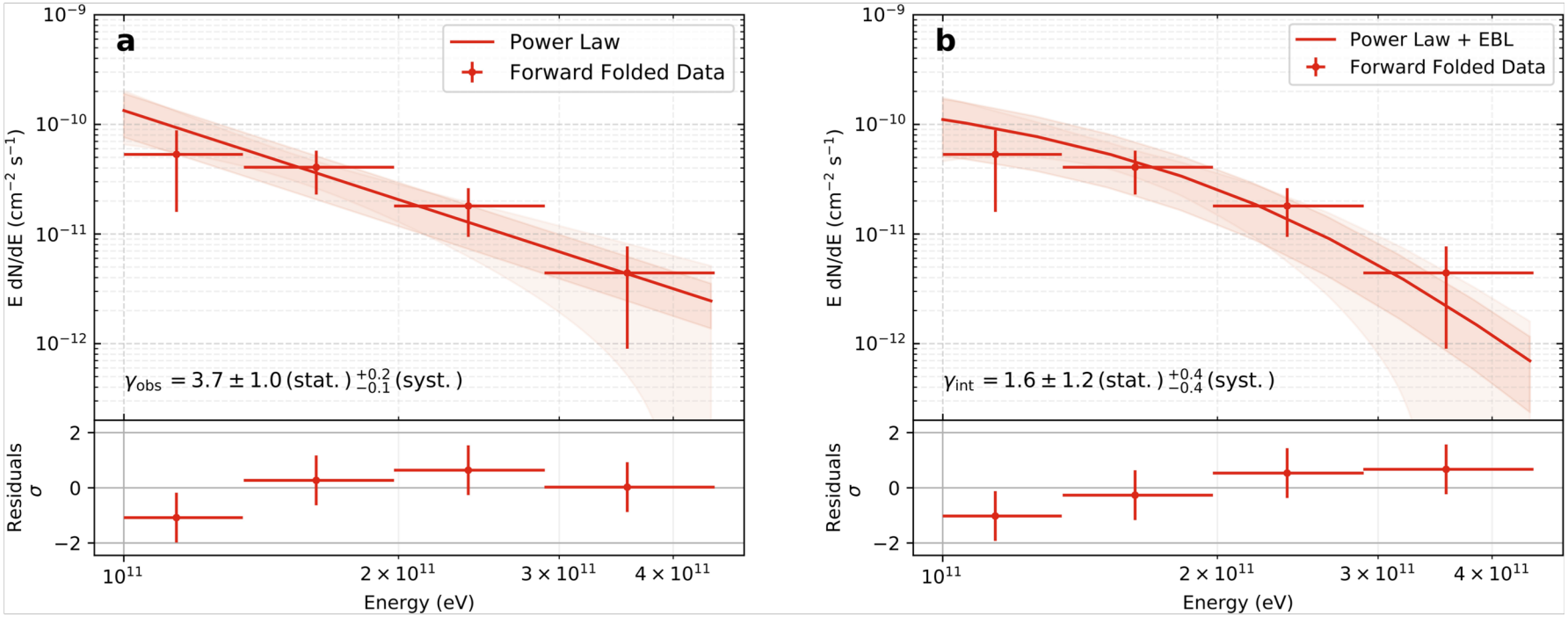

Extended Data Fig. 1 | VHE spectral fit of GRB 180720B. H.E.S.S. spectral fit to the measured emission in the energy range 100–440 GeV. **a**, Fit using a simple power-law model (with photon index γ_{obs}). **b**, Fit with a power-law model (with photon index γ_{int}) with EBL attenuation for a source at $z = 0.653$ (ref. [13]). In both cases the residual data points with 1σ uncertainties are obtained from the forward-folded method. The shaded areas show the statistical and systematic uncertainties in each fit (1σ confidence level). The bottom panels show the significance of the residuals between the fitted model and the data points.

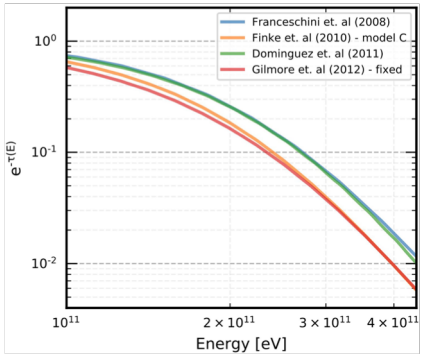

Extended Data Fig. 2 | EBL absorption coefficient. Absorption coefficient $e^{-\tau(E)}$ for a source emitting at a redshift of 0.653. The values are shown in the energy range of the detected emission of GRB 180720B (100–440 GeV) for the four EBL models considered[13,39–41].

A very-high-energy component deep in the γ-ray burst afterglow, H.E.S.S. collaboration; *Nature 575*, 464-467 (2019)

GRB180720B: VHE spectrum

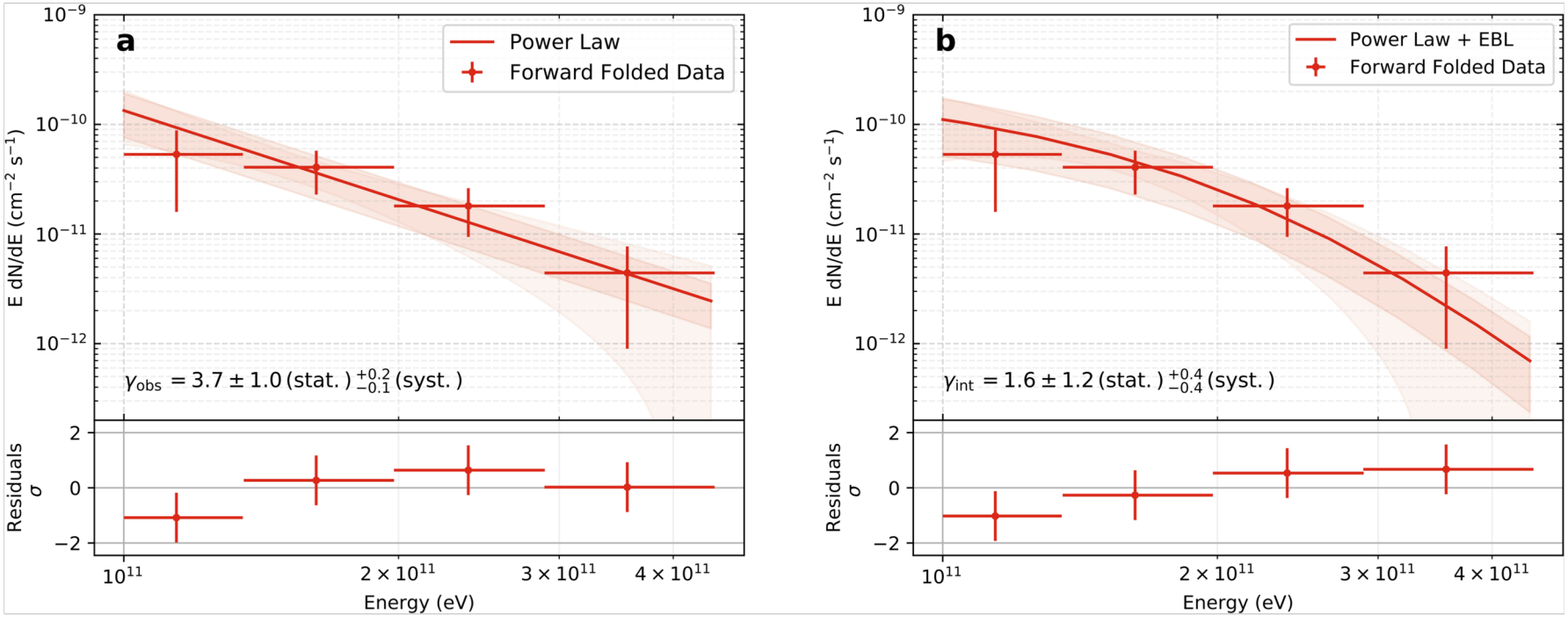

Extended Data Fig. 1 | VHE spectral fit of GRB 180720B. H.E.S.S. spectral fit to the measured emission in the energy range 100–440 GeV. **a**, Fit using a simple power-law model (with photon index γ_{obs}). **b**, Fit with a power-law model (with photon index γ_{int}) with EBL attenuation for a source at $z = 0.653$ (ref. [13]). In both cases the residual data points with 1σ uncertainties are obtained from the forward-folded method. The shaded areas show the statistical and systematic uncertainties in each fit (1σ confidence level). The bottom panels show the significance of the residuals between the fitted model and the data points.

Extended Data Table 1 | VHE spectral information from GRB 180720B

Spectral model	F_0 [$\times 10^{-10}$ cm^{-2} s^{-1} TeV^{-1}]	γ	E_0 [TeV]
$F_0 \times \left(\frac{E}{E_0}\right)^{-\gamma}$	$2.71 \pm 0.74\,^{+1.43}_{-1.16}$	$3.7 \pm 1.0\,^{+0.2}_{-0.1}$	0.154
$F_0 \times \left(\frac{E}{E_0}\right)^{-\gamma} \times e^{-\tau(z,E)}$	$7.52 \pm 2.03\,^{+4.53}_{-3.84}$	$1.6 \pm 1.2\,^{+0.4}_{-0.4}$	0.154
$F_0 \times \left(\frac{E}{E_0}\right)^{-2} \times e^{-\tau(z,E)}$	$16.12 \pm 4.37\,^{+10.59}_{-9.25}$	2.0 [Fixed]	0.105

Spectral parameters of the fits to the H.E.S.S. observed emission in the energy range 100–440 GeV. The intrinsic spectrum with $\gamma = 2.0$ (third row) is provided as a reference to the Fermi-LAT mean photon index detected in several other GRBs at high energies[14]. All reported uncertainties are statistical and systematic, in that order.

A very-high-energy component deep in the γ-ray burst afterglow, H.E.S.S. collaboration; *Nature 575*, 464-467 (2019)

GRB180720B: CTA detectability prospects

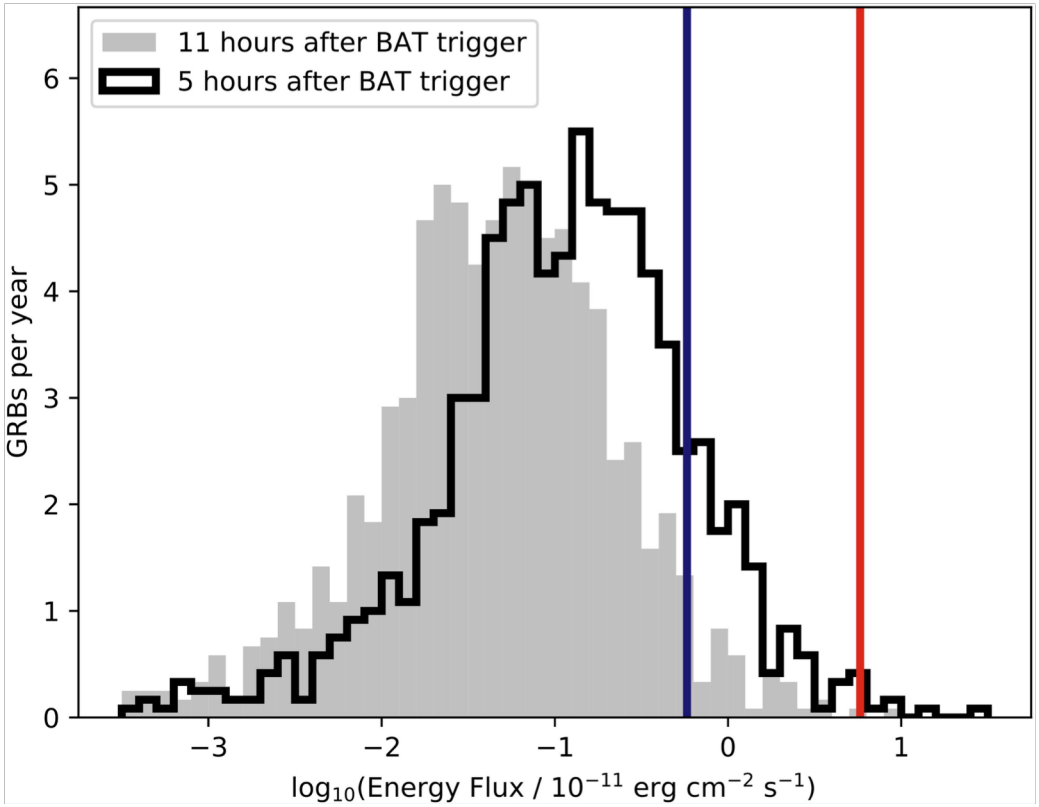

Extended Data Fig. 3 | CTA detectability prospects. Energy-flux distribution at 11 h and 5 h after the Swift-BAT trigger for all the GRBs observed by Swift-XRT per year. The blue vertical line shows the expected sensitivity of CTA, assuming the detection of fluxes 10 times fainter than that of GRB 180720B. The energy flux of GRB 180720B is indicated by the red vertical line.

> 3 afterglows at VHE/year with CTA?

(assumes VHE flux = XRT flux as for 1708720B…)

A very-high-energy component deep in the γ-ray burst afterglow, H.E.S.S. collaboration; *Nature 575*, 464-467 (2019)

GRB180720B: interpretation

- **Afterglow / Forward Shock**
- **Dominant: accelerated electrons**
  - Direct synchrotron: unlikely

    $E_{\rm sync}^{\rm max} = 9\Gamma mc^2/(4\alpha_{\rm F}) \approx 100\Gamma\,{\rm MeV}$

    Needs Γ>1000 at 10h!

  - **SSC**
    (VHE photons produced by
    IC scatterings of IR-UV photons
    by electrons at the highest energy)

Klein-Nishina attenuation?
$E \gtrsim 50(\Gamma/20)^2[E_{\rm t}/(1\,{\rm keV})]^{-1}\,{\rm GeV}.$

Detailed modelling is required…

- Weak proton emission?

Synchrotron (« burnoff ») limit

Very efficient acceleration:

$$t_{\rm syn}(\gamma_{\rm max}) \sim t_{\rm acc} \sim \frac{R_{\rm L}}{c}$$

with

$$t_{\rm syn}(\gamma) \propto B^{-2}\gamma^{-1}$$

$$t_{\rm acc}(\gamma) \sim \frac{R_{\rm L}}{c} \propto \gamma B^{-1}$$

then $\gamma_{\rm max} \propto B^{-1/2}$

$$E_{\rm syn}(\gamma_{\rm max}) \propto \Gamma B \gamma_{\rm max}^2 \propto \Gamma$$

KN limit

$$\gamma h\nu' > m_{\rm e}c^2$$

$h\nu'$: seed photon γ: electron

GRB190114C: significance of gamma-rays

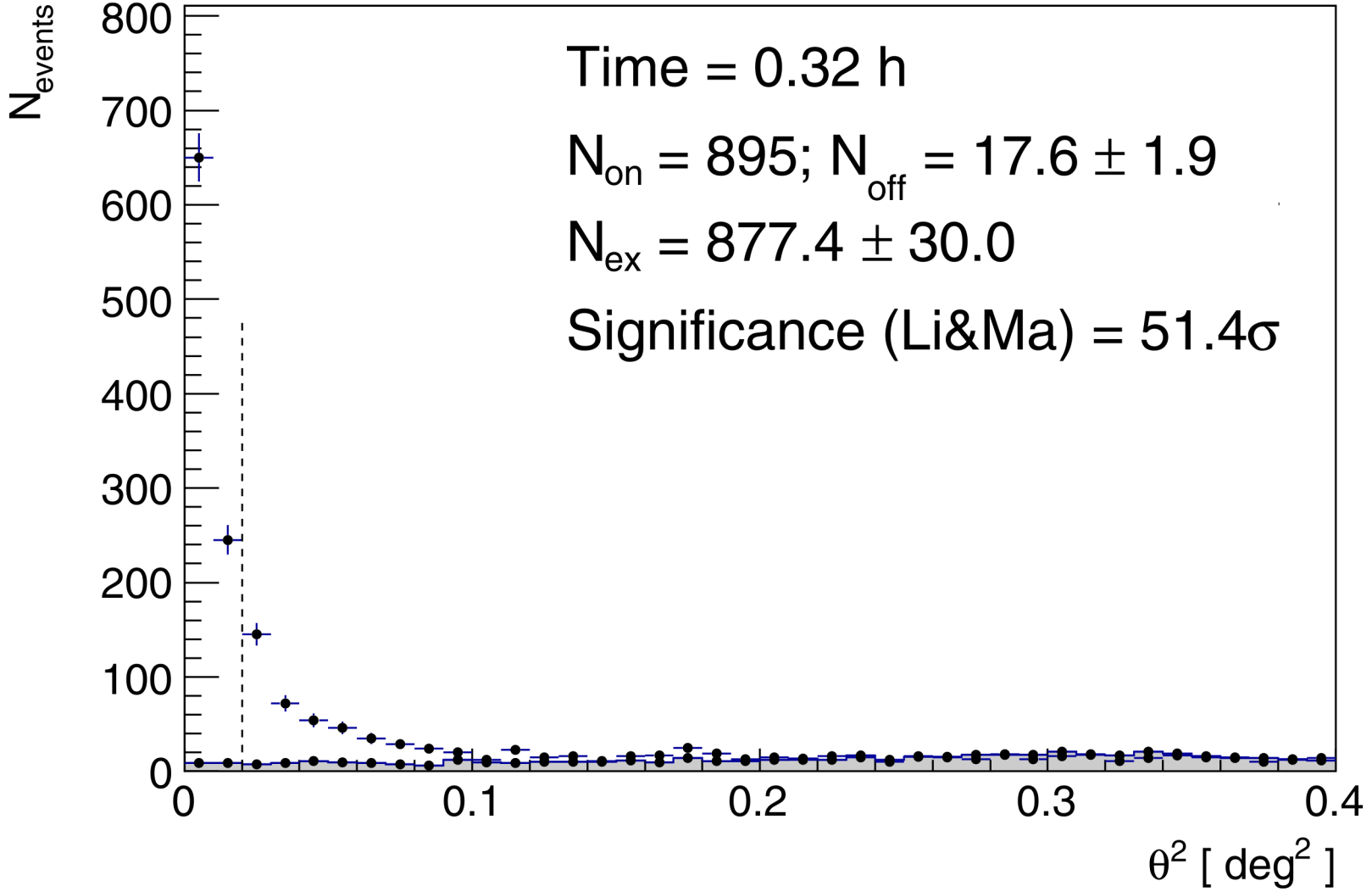

Extended Data Fig. 2 | Significance of the γ-ray signal between T_0 + 62 s and T_0 + 1,227 s for GRB 190114C. Distribution of the squared angular distance, θ^2, for the MAGIC data (points) and background events (grey shaded area). θ^2 is defined as the squared angular distance between the nominal position of the source and the reconstructed arrival direction of the events. The dashed vertical line represents the value of the cut on θ^2. This defines the signal region, where the number of events coming from the source (N_{on}) and from the background (N_{off}) are computed. The errors for 'on' events are derived from Poissonian statistics. From N_{on} and N_{off}, the number of excess events (N_{ex}) is computed. The significance is calculated using the Li & Ma method[42].

Teraelectronvolt emission from the γ-ray burst GRB 190114C, MAGIC collaboration; *Nature* 575, 455-458 (2019)

GRB 190114C (MAGIC)

GRB190114C: VHE photons

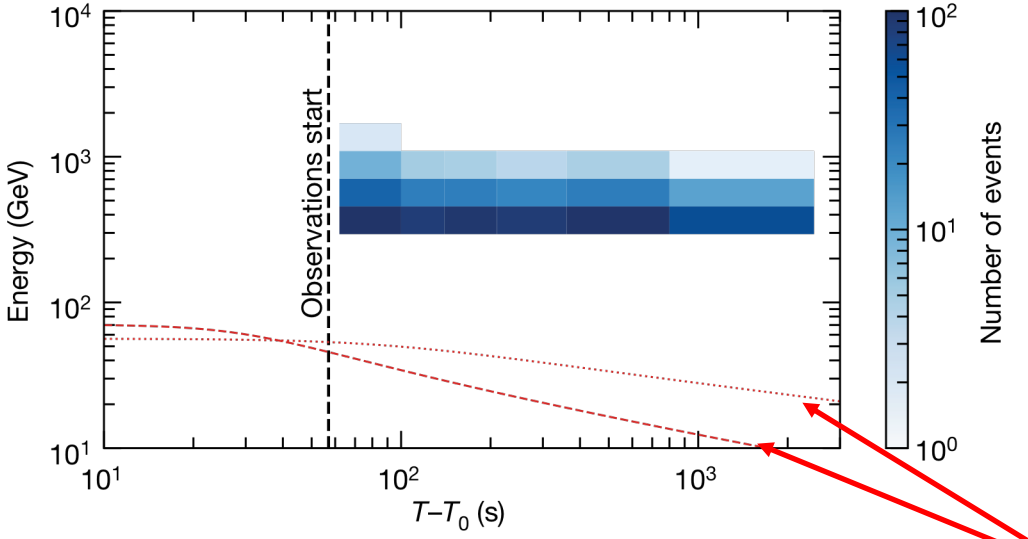

synchrotron limit
« standard » AG theory

Fig. 3 | Distribution of the number of teraelectronvolt-band γ-rays in time and energy for GRB 190114C. The number of events in each bin of energy and time are colour-coded (Methods). The vertical line indicates the beginning of the data acquisition. The curves show the expected maximum photon energy $\varepsilon_{\mathrm{syn,max}}$ of electron synchrotron radiation in the standard afterglow theory for two extreme cases giving high values of $\varepsilon_{\mathrm{syn,max}}$. The dotted curve corresponds to an isotropic-equivalent blast-wave kinetic energy of $E_{\mathrm{k,aft}} = 3 \times 10^{55}$ erg and a homogeneous external medium with density $n = 0.01\,\mathrm{cm}^{-3}$; the dashed curve corresponds to $E_{\mathrm{k,aft}} = 3 \times 10^{55}$ erg and an external medium describing a progenitor stellar wind with a density profile of $n(R) = AR^{-2}$ as a function of radius R, where $A = 3 \times 10^{33}\,\mathrm{cm}^{-1}$ (Methods).

Teraelectronvolt emission from the γ-ray burst GRB 190114C, MAGIC collaboration; *Nature* 575, 455-458 (2019)

GRB190114C: lightcurve XRT-LAT-MAGIC

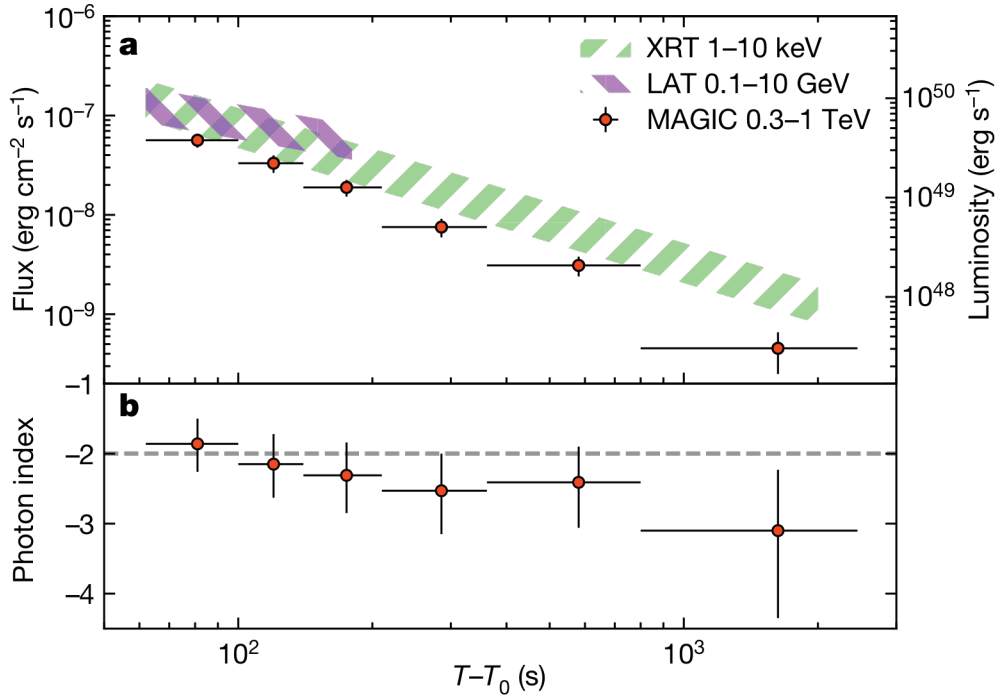

Fig. 1 | Light curves in the kiloelectronvolt, gigaelectronvolt and teraelectronvolt bands, and spectral evolution in the teraelectronvolt band for GRB 190114C. a, Light curves in units of energy flux (left axis) and apparent luminosity (right axis), for MAGIC at 0.3–1 TeV (red symbols), the Fermi Large Area Telescope (LAT) at 0.1–10 GeV (purple band) and the Swift X-ray Telescope (XRT) at 1–10 keV (green band). For the MAGIC data, the intrinsic flux is shown, corrected for EBL attenuation[25] from the observed flux. **b**, Temporal evolution of the power-law photon index, determined from time-resolved intrinsic spectra. The horizontal dashed line indicates the value −2. The errors shown in both panels are statistical only (one standard deviation).

$\alpha_{MAGIC} \sim -1.6$

Early times: MAGIC vs BAT

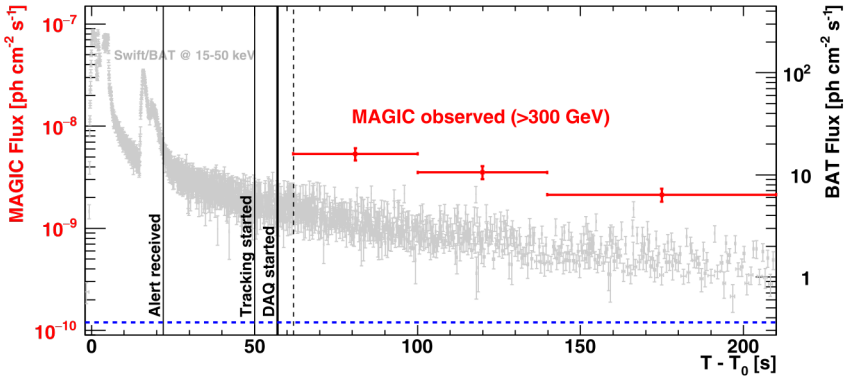

Extended Data Fig. 1 | Light curves in the teraelectronvolt and kiloelectronvolt bands for GRB 190114C. Photon flux light curve above 0.3 TeV measured by MAGIC (red; from T_0 + 62 s to T_0 + 210 s), compared with that between 15 keV and 50 keV measured by Swift-BAT[23] (grey; from T_0 to T_0 + 210 s) and the photon flux above 0.3 TeV of the Crab Nebula (blue dashed line). The errors on the MAGIC photon fluxes correspond to one standard deviation. Vertical lines indicate the times when the alert was received (T_0 + 22 s) by MAGIC, when the tracking of the GRB by the telescopes started (T_0 + 50 s), when the data acquisition started (T_0 + 57 s), and when the data acquisition system (DAQ) became stable (T_0 + 62 s; dotted line).

Teraelectronvolt emission from the γ-ray burst GRB 190114C, MAGIC collaboration; *Nature* 575, 455-458 (2019)

GRB190114C: afterglow

Host = spiral galaxy

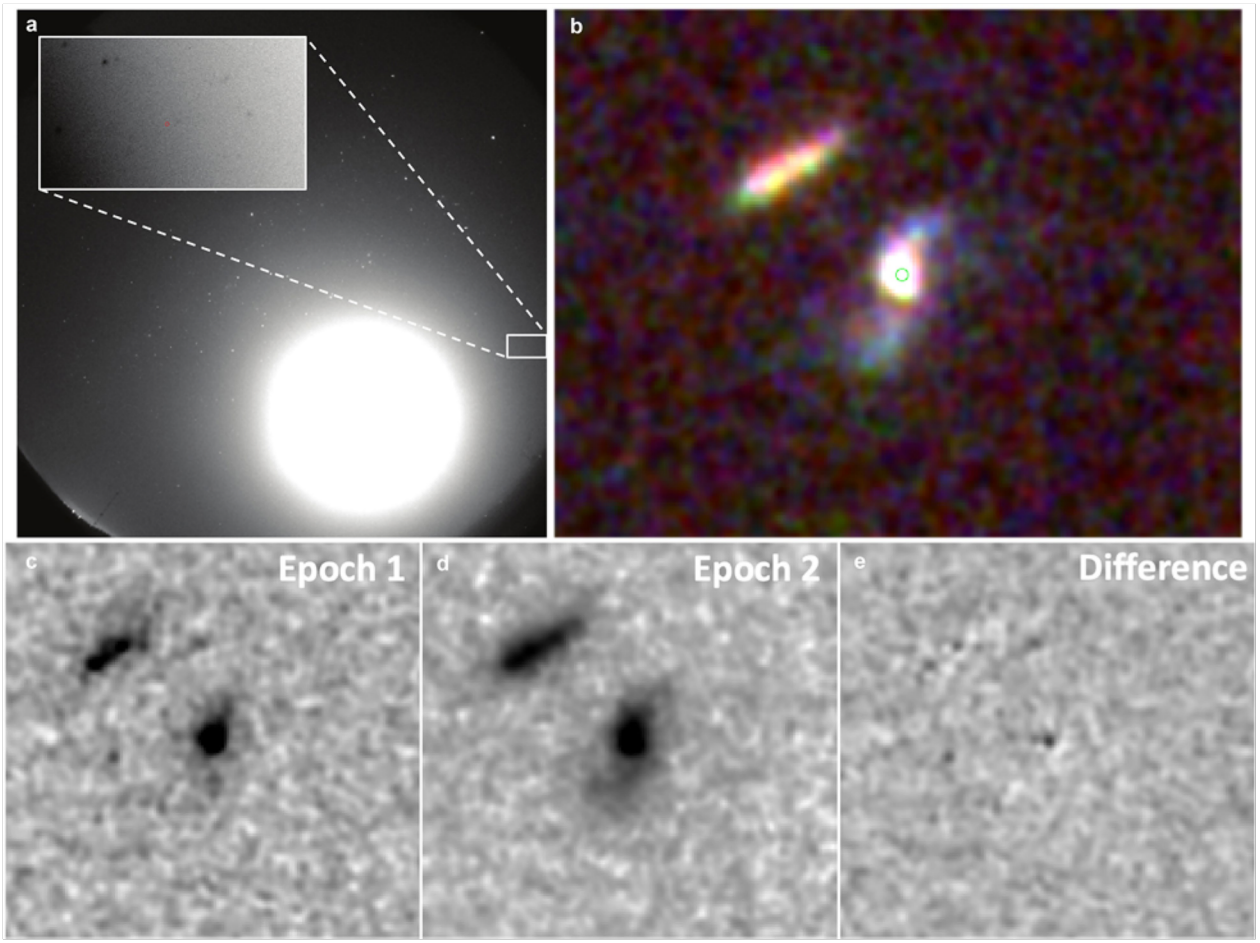

Extended Data Fig. 4 | Images of the localization region of GRB 190114C. **a**, All-sky image captured with the CASANDRA-1 camera at the BOOTES-1 station. The image (30 s exposure, unfiltered) was taken at T_0 + 14.8 s, and was severely affected by the moon. At the GRB190114C location (red dot) no prompt optical emission is detected. Inset, magnification (inverted colours) containing a 10′-diametercircle centred on the optical position. **b**, Three-colour image of the host of GRB 190114C, obtained with the HST. The host galaxy is a spiral galaxy, and the green circle indicates the location of the transient close to its host nucleus. The image is 8″ across; north is up and east is to the left. **c**–**e**, Images of the GRB 190114C field taken with the HST, obtained with the F850LP filter (covering roughly the region from 800 to 1,100 nm). Two epochs, 11 February and 12 March 2019, are shown (images are 4″ across); the right-most image is the result of the difference image. A faint transient is visible close to the nucleus of the galaxy, and we identify this as the late-time afterglow of the burst.

Observation of inverse Compton emission from a long γ-ray burst, MAGIC collaboration; *Nature* 575, 459-463 (2019)

GRB190114C: multi-λ lightcurve

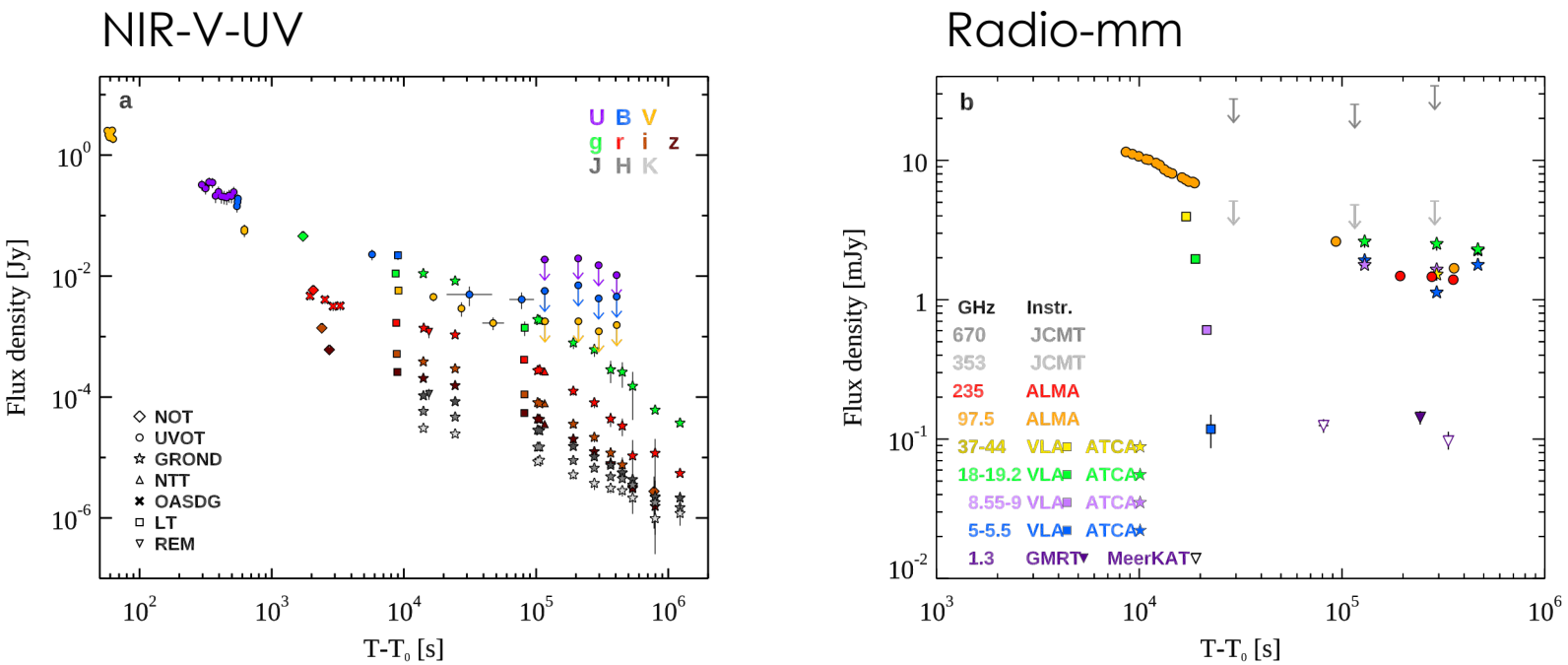

Extended Data Fig. 3 | Afterglow light curves of GRB 190114C. Flux density at different frequencies as a function of the time since the initial burst, $T - T_0$. **a**, Observation in the NIR, optical and UV bands. The flux has been corrected for extinction in the host and in our Galaxy. The contribution of the host galaxy and its companion has been subtracted. Fluxes have been rescaled (except for the r-band filter). **b**, Radio and submillimetre observations from 1.3 GHz to 670 GHz. 'Instr.', instrument.

Observation of inverse Compton emission from a long γ-ray burst, MAGIC collaboration; *Nature* 575, 459-463 (2019)

GRB190114C: multi-λ lightcurve

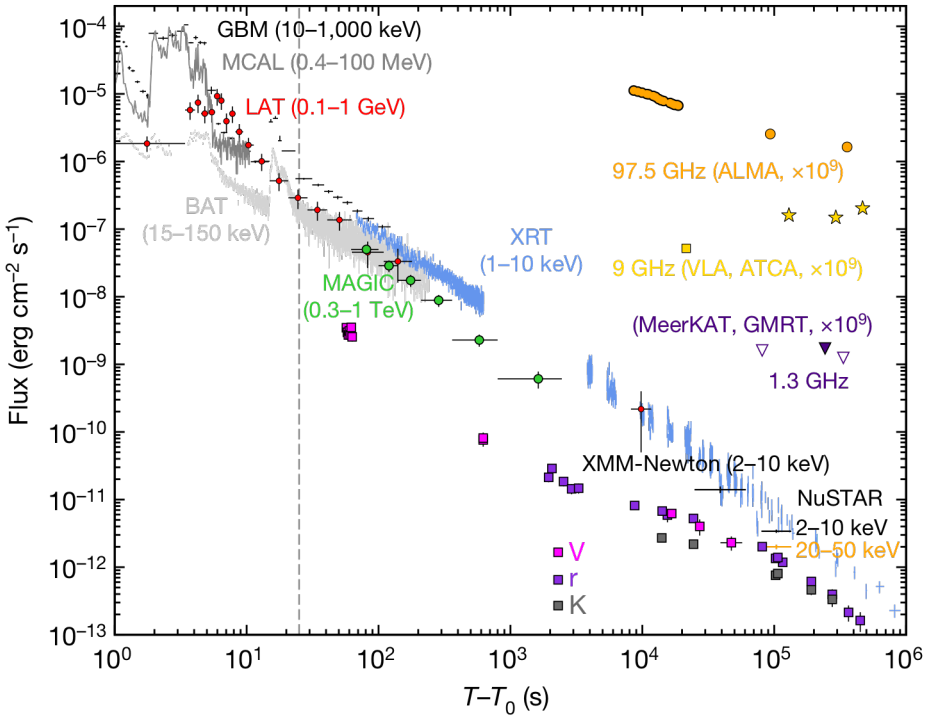

Fig. 1 | Multi-wavelength light curves of GRB 190114C. Energy flux at different wavelengths, from radio to γ-rays, versus time after the BAT trigger, at T_0 = 20:57:03.19 universal time (UT) on 14 January 2019. The light curve for the energy range 0.3–1 TeV (green circles) is compared with light curves at lower frequencies. Those for VLA (yellow square), ATCA (yellow stars), ALMA (orange circles), GMRT (purple filled triangle) and MeerKAT (purple open triangles) have been multiplied by 10^9 for clarity. The vertical dashed line marks approximately the end of the prompt-emission phase, identified as the end of the last flaring episode. For the data points, vertical bars show the 1σ errors on the flux, and horizontal bars represent the duration of the observation. The fluxes in the V, r and K filters (pink, purple and grey filled squares, respectively) have been corrected for extinction in the host and in our Galaxy; the contribution from the host galaxy has been subtracted.

$\alpha_{10\text{-}1000\ keV}$ ~ -1.1 after 5-10 s

α_{XRT} ~ -1.4
α_{MAGIC} ~ -1.5

NIR-V (square symbols):
-Early: RS contribution?
-Then shallow decay/fast decay

Radio-mm:
-Early: RS contribution?
-Then ~cst flux

Observation of inverse Compton emission from a long γ-ray burst, MAGIC collaboration; *Nature* 575, 459-463 (2019)

GRB190114C: prompt lightcurve

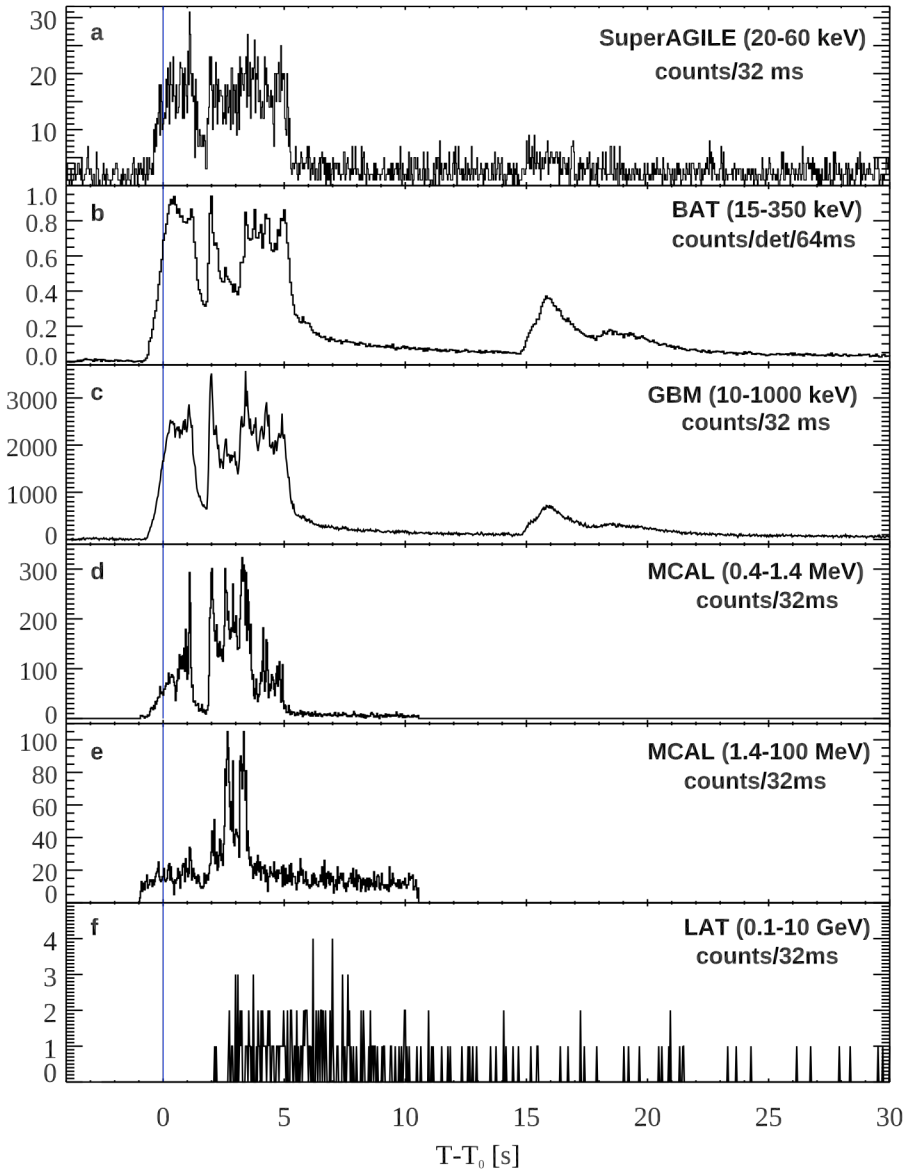

Extended Data Fig. 1 | Prompt-emission light curves for different detectors. **a**–**f**, Light curves for Super-AGILE (**a**; 20–60 keV), Swift-BAT (**b**; 15–150 keV), Fermi-GBM (**c**; 10–1,000 keV), AGILE-MCAL (**d**; 0.4–1.4 MeV), AGILE-MCAL (**e**; 1.4–100 MeV) and Fermi-LAT (**f**; 0.1–10 GeV). The light curve of AGILE-MCAL is split into two bands to show the energy dependence of the first peak. Error bars show 1σ statistical errors.

GRB190114C: VHE spectrum

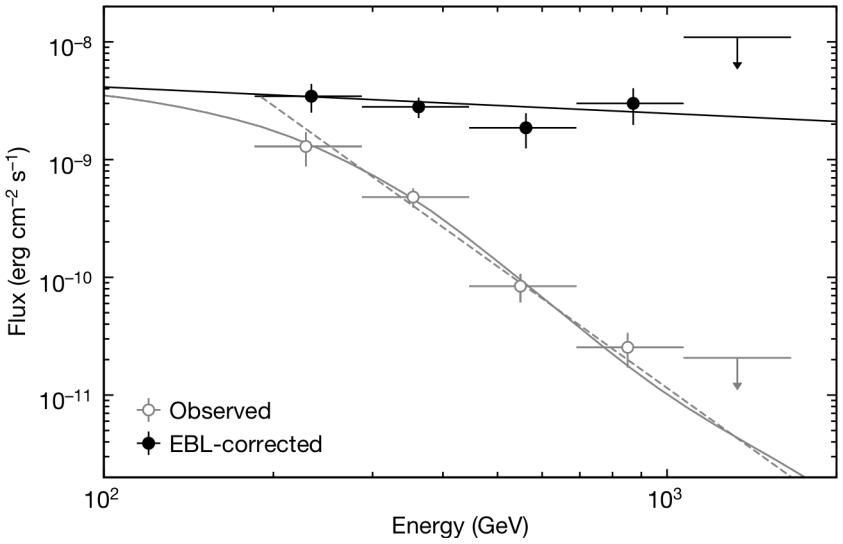

Fig. 2 | Spectrum above 0.2 TeV averaged over the period between T_0 + 62 s and T_0 + 2,454 s for GRB 190114C. Spectral-energy distributions for the spectrum observed by MAGIC (grey open circles) and the intrinsic spectrum corrected for EBL attenuation[25] (blue filled circles). The errors on the flux correspond to one standard deviation. The upper limits at 95% confidence level are shown for the first non-significant bin at high energies. Also shown is the best-fit model for the intrinsic spectrum (black curve) when assuming a power-law function. The grey solid curve for the observed spectrum is obtained by convolving this curve with the effect of EBL attenuation. The grey dashed curve is the forward-folding fit to the observed spectrum with a power-law function (Methods).

Photon index
~-2.2

Limits on systematics:

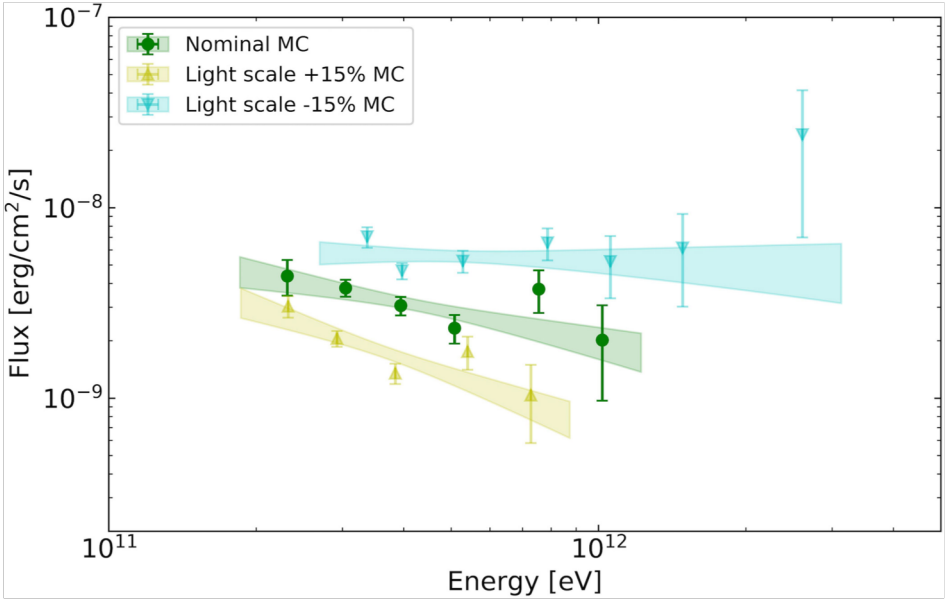

Extended Data Fig. 2 | MAGIC time-integrated SEDs in the time interval 62–2,400 s after T_0. The green (yellow, blue) points and band show the results of the Monte Carlo (MC) simulations for the nominal and the varied light scale cases (+15%, −15%), which define the limits of the systematic uncertainties. The contour regions are drawn from the 1σ error of their best-fit power-law functions. The vertical bars of the data points show the 1σ errors on the flux.

Teraelectronvolt emission from the γ-ray burst GRB 190114C, MAGIC collaboration; *Nature* 575, 455-458 (2019)

Observation of inverse Compton emission from a long γ-ray burst, MAGIC collaboration; *Nature* 575, 459-463 (2019)

GRB190114C: multi-λ spectrum

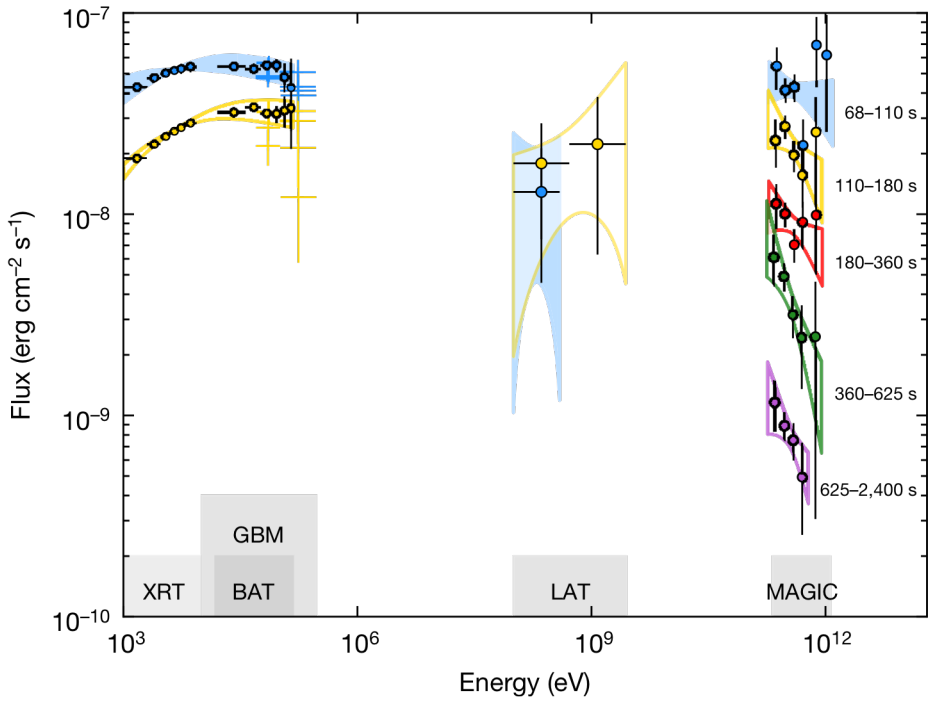

Fig. 2 | Multi-band spectra in the time interval 68–2,400 s. Five time intervals are considered: 68–110 s (blue), 110–180 s (yellow), 180–360 s (red), 360–625 s (green) and 625–2,400 s (purple). MAGIC data points have been corrected for attenuation caused by the EBL. Data from other instruments (Swift-XRT, Swift-BAT, Fermi-GBM and Fermi-LAT) are shown for the first two time intervals. For each time interval, LAT contour regions are shown, limiting the energy to the range in which photons are detected. MAGIC and LAT contour regions are drawn from the 1σ error of their best-fit power-law functions. For Swift data, the regions show the 90% confidence contours for the joint fit for XRT and BAT, obtained by fitting a smoothly broken power law to the data. Filled regions are used for the first time interval (68–110 s).

Two components (clear for the first two intervals)

Independent of the choice of an EBL model

SSC in external shock?

Observation of inverse Compton emission from a long γ-ray burst, MAGIC collaboration; *Nature* 575, 459-463 (2019)

GRB190114C: spectral evolution?

Extended Data Table 1 | Energy flux between 0.3 and 1 TeV in selected time bins for GRB 190114C

Time bin [seconds after T_0]	Energy flux [erg cm^{-2} s^{-1}]	Spectral index
62 – 100	$[5.64 \pm 0.90\,(\text{stat})\,^{+3.24}_{-3.22}\,(\text{sys})] \cdot 10^{-8}$	$-1.86\,^{+0.36}_{-0.40}\,(\text{stat})\,^{+0.12}_{-0.21}\,(\text{sys})$
100 – 140	$[3.31 \pm 0.67\,(\text{stat})\,^{+2.71}_{-1.84}\,(\text{sys})] \cdot 10^{-8}$	$-2.15\,^{+0.43}_{-0.48}\,(\text{stat})\,^{+0.25}_{-0.32}\,(\text{sys})$
140 – 210	$[1.89 \pm 0.36\,(\text{stat})\,^{+1.72}_{-0.94}\,(\text{sys})] \cdot 10^{-8}$	$-2.31\,^{+0.47}_{-0.54}\,(\text{stat})\,^{+0.15}_{-0.22}\,(\text{sys})$
210 – 361.5	$[7.54 \pm 1.60\,(\text{stat})\,^{+6.46}_{-4.41}\,(\text{sys})] \cdot 10^{-9}$	$-2.53\,^{+0.53}_{-0.62}\,(\text{stat})\,^{+0.22}_{-0.24}\,(\text{sys})$
361.5 – 800	$[3.10 \pm 0.70\,(\text{stat})\,^{+1.20}_{-2.36}\,(\text{sys})] \cdot 10^{-9}$	$-2.41\,^{+0.51}_{-0.65}\,(\text{stat})\,^{+0.27}_{-0.34}\,(\text{sys})$
800 – 2454	$[4.54 \pm 2.04\,(\text{stat})\,^{+7.66}_{-1.96}\,(\text{sys})] \cdot 10^{-10}$	$-3.10\,^{+0.87}_{-1.25}\,(\text{stat})\,^{+0.75}_{-0.24}\,(\text{sys})$
62 – 2454 (time integrated)	-	$-2.22\,^{+0.23}_{-0.25}\,(\text{stat})\,^{+0.21}_{-0.26}\,(\text{sys})$

Values listed correspond to the light curve in Fig. 1. For each time bin, columns represent the start and end time of the bin, the EBL-corrected energy flux in the 0.3–1 TeV range, and the best-fit spectral photon indices. The last row reports the value of the intrinsic spectral index for the time-integrated spectrum (Fig. 2). The reported statistical errors (stat) correspond to one standard deviation, whereas systematic errors (sys) are derived from the variation of the light scale by ±15% (see Methods).

Extended Data Table 2 | Number of γ-rays from GRB 190114C in the highest-energy bins

E_{min} [TeV]	E_{max} [TeV]	Model counts in $[E_{min}; E_{max}]$	Significance above E_{min}
0.71	1.10	25.4	5.8
1.10	1.70	4.1	2.5
1.70	2.64	0.9	1.5
2.64	4.09	0.1	0.1

The number of γ-ray counts was estimated from the MAGIC data using the power-law spectral model for the time interval between T_0 + 62 s and T_0 + 1,227 s.

Effect of EBL model:

Extended Data Table 4 | Spectral indices for different EBL models

Time bin [seconds after T_0]	D11	F08	FI10	G12
62 – 100	$-1.86^{+0.36}_{-0.40}$	$-2.04^{+0.36}_{-0.40}$	$-1.81^{+0.36}_{-0.40}$	$-1.95^{+0.36}_{-0.39}$
100 – 140	$-2.15^{+0.43}_{-0.48}$	$-2.32^{+0.43}_{-0.48}$	$-2.09^{+0.43}_{-0.48}$	$-2.23^{+0.42}_{-0.48}$
140 – 210	$-2.31^{+0.47}_{-0.54}$	$-2.48^{+0.47}_{-0.54}$	$-2.25^{+0.47}_{-0.54}$	$-2.39^{+0.47}_{-0.53}$
210 – 361.5	$-2.53^{+0.53}_{-0.62}$	$-2.69^{+0.52}_{-0.61}$	$-2.46^{+0.52}_{-0.61}$	$-2.60^{+0.52}_{-0.61}$
361.5 – 800	$-2.41^{+0.51}_{-0.65}$	$-2.58^{+0.51}_{-0.64}$	$-2.34^{+0.51}_{-0.64}$	$-2.49^{+0.51}_{-0.64}$
800 – 2454	$-3.10^{+0.87}_{-1.25}$	$-3.20^{+0.83}_{-1.20}$	$-2.96^{+0.83}_{-1.20}$	$-3.08^{+0.82}_{-1.19}$
62 – 2454 (time integrated)	$-2.22^{+0.23}_{-0.25}$	$-2.39^{+0.23}_{-0.25}$	$-2.15^{+0.23}_{-0.25}$	$-2.29^{+0.23}_{-0.24}$

Teraelectronvolt emission from the γ-ray burst GRB 190114C, MAGIC collaboration; *Nature* 575, 455-458 (2019)

GRB190114C: spectral evolution?

Extended Data Table 1 | MAGIC spectral-fit parameters for GRB 190114C

Time bin [seconds after T_0]	Normalisation [$\mathrm{TeV^{-1}\,cm^{-2}\,s^{-1}}$]	Photon index	Pivot energy [GeV]
62 – 90	$1.95^{+0.21}_{-0.20} \cdot 10^{-7}$	$-2.17^{+0.34}_{-0.36}$	395.5
68 – 180	$1.10^{+0.09}_{-0.08} \cdot 10^{-7}$	$-2.27^{+0.24}_{-0.25}$	404.7
180 – 625	$2.26^{+0.21}_{-0.20} \cdot 10^{-8}$	$-2.56^{+0.27}_{-0.29}$	395.5
68 – 110	$1.74^{+0.16}_{-0.15} \cdot 10^{-7}$	$-2.16^{+0.29}_{-0.31}$	386.5
110 – 180	$8.59^{+0.95}_{-0.91} \cdot 10^{-8}$	$-2.51^{+0.37}_{-0.41}$	395.5
180 – 360	$3.50^{+0.38}_{-0.36} \cdot 10^{-8}$	$-2.36^{+0.34}_{-0.37}$	395.5
360 – 625	$1.65^{+0.23}_{-0.23} \cdot 10^{-8}$	$-3.16^{+0.48}_{-0.54}$	369.1
625 – 2400	$3.52^{+0.47}_{-0.47} \cdot 10^{-9}$	$-2.80^{+0.48}_{-0.54}$	369.1
62 – 2400 (Nominal MC)	$1.07^{+0.08}_{-0.07} \cdot 10^{-8}$	$-2.51^{+0.20}_{-0.21}$	423.8
62 – 2400 (Light scale +15% MC)	$7.95^{+0.58}_{-0.56} \cdot 10^{-9}$	$-2.91^{+0.23}_{-0.25}$	369.1
62 – 2400 (Light scale -15% MC)	$1.34^{+0.09}_{-0.09} \cdot 10^{-8}$	$-2.07^{+0.18}_{-0.19}$	509.5

For each time bin, the table shows the start and end time of the bin, the normalization factor of the EBL-corrected differential flux at the pivot energy with statistical errors, photon indices with statistical errors, and the pivot energy of the fit (fixed).

?

Observation of inverse Compton emission from a long γ-ray burst, MAGIC collaboration; *Nature* 575, 459-463 (2019)

GRB190114C: observed vs expected number of events?

Extended Data Table 3 | Observed and expected number of events in estimated-energy bins for GRB 190114C

$E_{est,min}$ [TeV]	$E_{est,max}$ [TeV]	Observed photons	Expected photons
0.19	0.29	155 ± 13	219 ± 73
0.29	0.46	598 ± 26	564 ± 53
0.46	0.71	154 ± 13	180 ± 16
0.71	1.10	32 ± 6	28 ± 3
1.10	1.70	6.0 ± 2.9	5.6 ± 0.4
1.70	2.64	2.3 ± 1.8	1.2 ± 0.1

The number of expected events is calculated from the intrinsic spectrum power-law model, by convolving it with the effect of EBL attenuation and the instrument response function of the telescope for these large zenith angles. The energy binning in estimated energy matches the one in true energy (after unfolding) shown in Fig. 2 and Extended Data Table 2. The large uncertainty in the number of expected events in the lowest-energy bin is dominated by the uncertainty in the very low effective area of the telescopes close to the energy threshold of this analysis. The numbers reported in this table cannot be used directly for any physical inference. The measured spectrum needs to be first unfolded using the energy migration matrix[21].

Teraelectronvolt emission from the γ-ray burst GRB 190114C, MAGIC collaboration; *Nature* 575, 455-458 (2019)

MAGIC: other GRBs?

Extended Data Table 5 | List of GRBs observed under adequate technical and weather conditions by MAGIC with $z < 1$ and $T_{delay} < 1$ h

Event	redshift	T_{delay} (s)	Zenith angle (deg)
GRB 061217	0.83	786.0	59.9
GRB 100816A	0.80	1439.0	26.0
GRB 160821B	0.16	24.0	34.0
GRB 190114C	0.42	58.0	55.8

The zenith angle at the beginning of the observations is reported in the last column. All GRBs except GRB 061217 were observed in stereoscopic mode. GRB 061217, GRB 100816A and GRB 160821B are short GRBs, whereas GRB 190114C is a long GRB. Observations of a few other long GRBs with the same criteria were also conducted but are not listed here, because they were affected by technical problems or adverse observing conditions.

Low z + « suitable » observing conditions rather than special intrinsic properties

Teraelectronvolt emission from the γ-ray burst GRB 190114C, MAGIC collaboration; *Nature* 575, 455-458 (2019)

GRB190114C: interpretation

- **Again: Afterglow / Forward Shock**
- **Subdominant prompt component at early times?**
  Paper says : <20% during first 100 s (IS,rec) – Short discussion: photosphere

  Duration of the prompt phase? T_{90} ~100-300 s (1st paper); duration ∞ 25 s (2nd paper)
  Onset of the afterglow phase: ~ 5-10 s ?

- **Dominant: accelerated electrons**
  up to LAT: synchrotron ; MAGIC: SSC $\varepsilon_{\rm syn,max} \approx 100 (\Gamma_{\rm b}/1{,}000)\ {\rm GeV},$

- **SSC component is energetically important**

- Weak proton emission?

  - Proton synchrotron: $\varepsilon_{\rm psyn,max} = (7.6\ {\rm GeV}) \eta^{-2} \epsilon_{\rm B}^{3/2} (n_0 E_{\rm k,53})^{3/4} t_{\rm s}^{-1/4} (1+z)^{-3/4}$

    slope –(p+1)/2
    above $\nu_{\rm m}$ $\varepsilon_{\rm m} = (3.7\times10^{-3}\ {\rm eV}) \xi_{\rm p}^{-2} \epsilon_{\rm p}^{2} \epsilon_{\rm B}^{1/2} E_{\rm k,53}^{1/2} t_{\rm s}^{-3/2} (1+z)^{1/2}$

    $f(\varepsilon=\varepsilon_{\rm m}) = (1.3\times10^{-28}\ {\rm erg\ cm^{-2}\ s^{-1}\ Hz^{-1}}) \times \xi_{\rm p} \epsilon_{\rm B}^{1/2} n_0^{1/2} E_{\rm k,53} D_{28}^{-2} (1+z)$

    $F(\varepsilon = 1\ {\rm TeV}) = (1.1\times10^{-16}\ {\rm erg\ cm^{-2}\ s^{-1}}) \times \epsilon_{\rm p}^{2} \xi_{\rm p}^{-1} \epsilon_{\rm B} n_0^{1/2} E_{\rm k,53}^{3/2} D_{28}^{-2} t_{\rm s}^{-3/2} (1+z)^{3/2}$

    $\Rightarrow n_0^{1/2} E_{\rm k,53}^{3/2} \gtrsim 10^{11}$ at 100 s !

GRB190114C: model

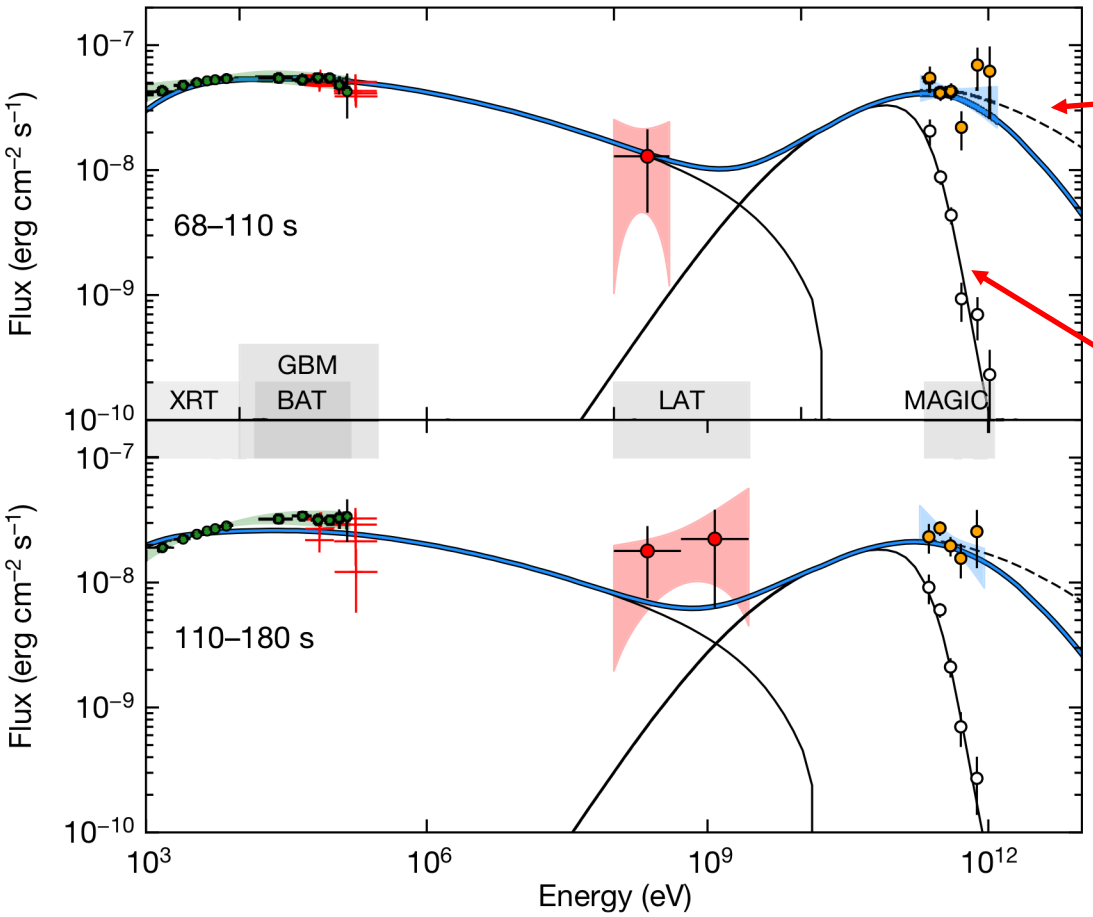

without γγ

with EBL attenuation

Fig. 3 | Modelling of the broadband spectra in the time intervals 68–110 s and 110–180 s. Thick blue curve, modelling of the multi-band data in the synchrotron and SSC afterglow scenario. Thin solid lines, synchrotron and SSC (observed spectrum) components. Dashed lines, SSC when internal γ–γ opacity is neglected. The adopted parameters are: $s = 0$, $\varepsilon_e = 0.07$, $\varepsilon_B = 8 \times 10^{-5}$, $p = 2.6$, $n_0 = 0.5$ and $E_k = 8 \times 10^{53}$ erg; see Methods. Empty circles show the observed MAGIC spectrum, that is, uncorrected for attenuation caused by the EBL. Contour regions and data points are as in Fig. 2.

GRB190114C: model

Afterglow: external shock

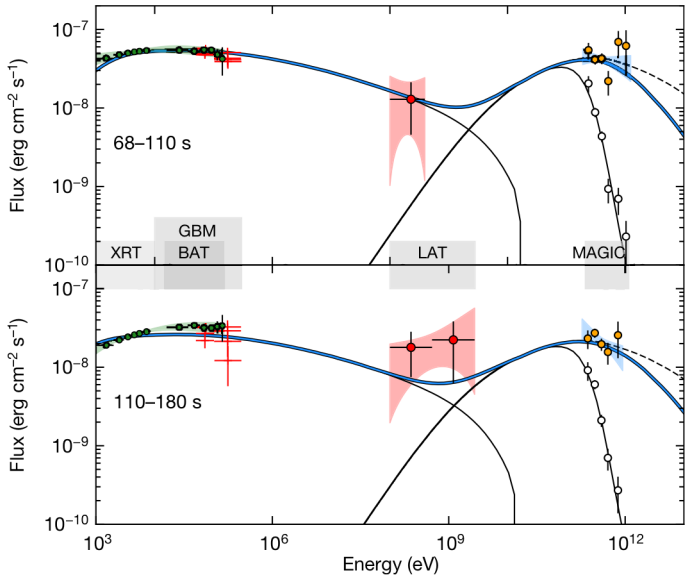

Onset ~ 5-10 s
Initial Lorentz factor ~ 300-700
Lorentz factor at 100 s ~150

-Syn peak at ~10 keV
-IC peak at < TeV
(flat spectrum)

Then: $\frac{4}{3}\gamma_{\rm m}^2 \sim \frac{200\,{\rm GeV}}{10\,{\rm keV}} \sim 2\,10^7$

$\gamma_{\rm m} \sim 4\,10^3$ (2 10^3)

Synchrotron peak: $h\nu_{\rm m} \simeq 30\,{\rm eV}\,\frac{\Gamma}{150}\frac{B}{1\,{\rm G}}\left(\frac{\gamma_{\rm m}}{4\,10^3}\right)^2$ Then: $B \sim 400\,{\rm G}$

Problem: - low electron Lorentz factor: low ε_e
- high magnetic field: high ε_B
- **Then: low ε_e / ε_B implies a low efficiency of SSC…**

This leads to a more complex model when the SSC peak is affected by KN and $\gamma\gamma$.

GRB190114C: model

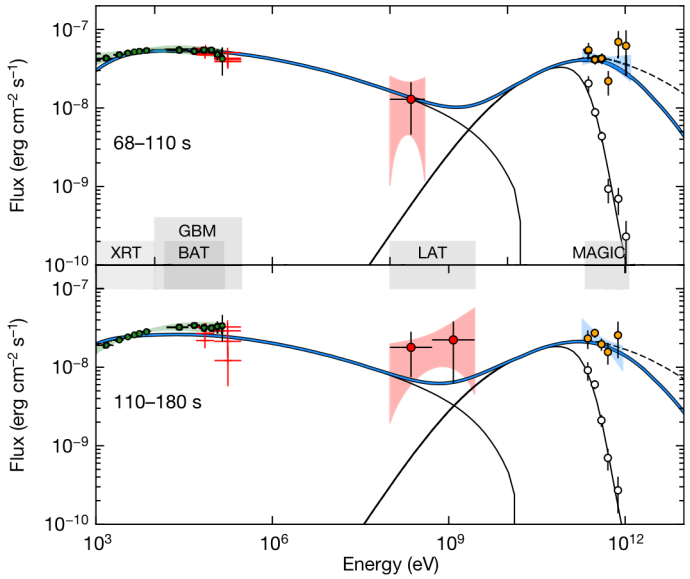

Detailed model:

Kinetic energy > 3 10^{53} erg
Efficiency of prompt phase > 50%

Radius ~ (8-20) 10^{16} cm at 100 s

Microphysics:
ε_e ~ 0.05-0.15 ; p ~ 2.4-2.6 ; γ_m ~ (0.8-2) 10^4 at 100 s
ε_B ~ 0.00005-0.001 ; B ~ 0.5-5 G at 100 s

$\varepsilon_e >> \varepsilon_B$: efficient SSC
At 100 s: comparable powers syn and IC

Exernal medium:
- Wind does not work
- Uniform: n_{ext} ~ 0.5-5 cm^{-3}

GRB190114C: model

– ν_m crosses the X-rays at ~10^2 s.
– ν_m crosses the optical band at ~10^5 s.

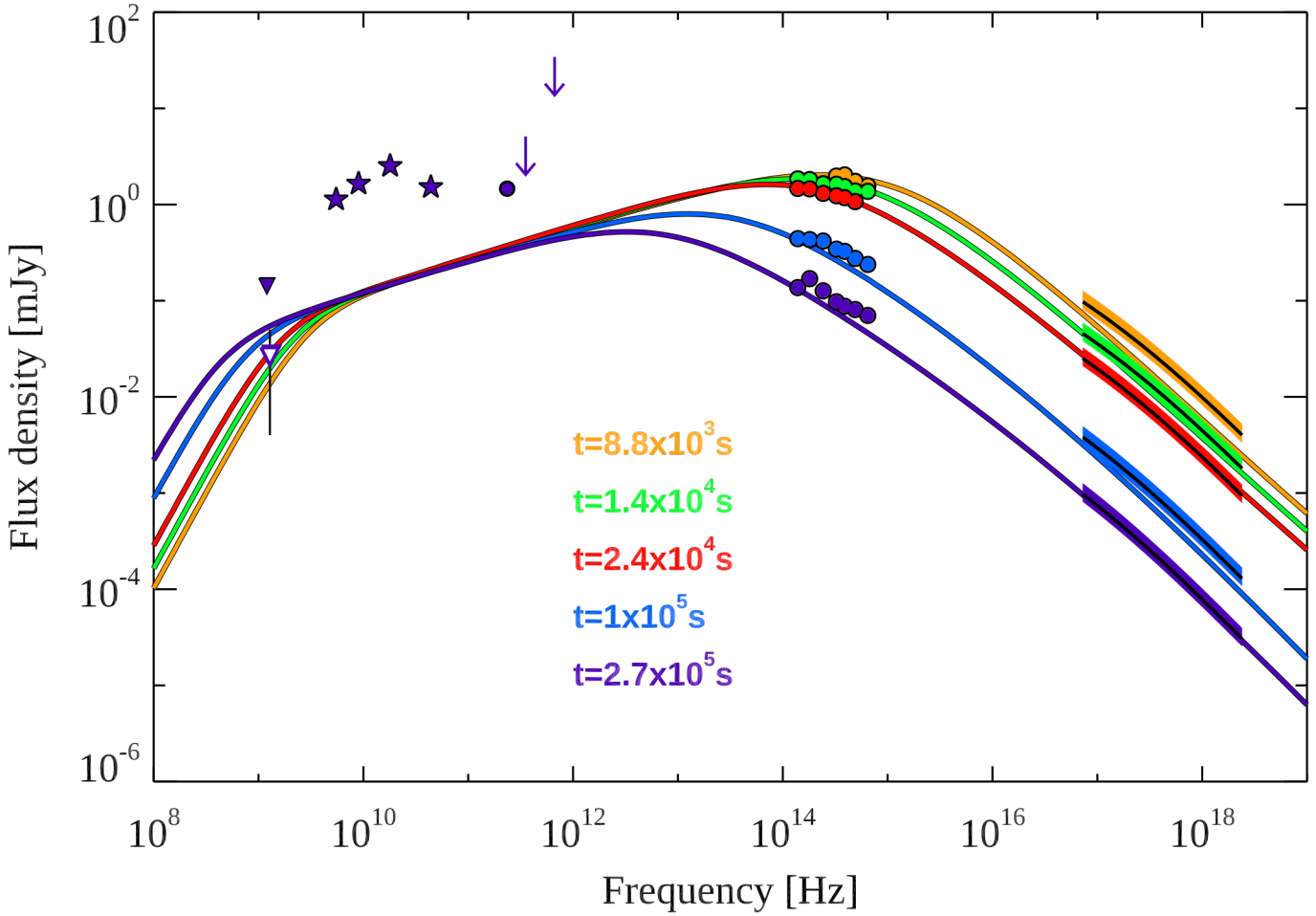

Extended Data Fig. 6 | SEDs from radio frequencies to X-rays at different epochs. The synchrotron frequency ν_m crosses the optical band, moving from higher to lower frequencies. The break between 10^8 and 10^{10} Hz is caused by the self-absorption synchrotron frequency, ν_{sa}. Optical (X-ray) data have been corrected for extinction (absorption). The data points are taken from the following telescopes (from lower to higher frequencies): filled and empty triangle symbols, GMRT and MeerKAT; stars, ATCA; violet filled circle, ALMA, down arrows, JCMT 1σ upper limits; filled circles, LT (yellow) and GROND (all the other colours). Error bars for all data points define the 1σ error. Coloured stripes show the best fit of the XRT data extrapolated to the time of each SED. Their vertical width is obtained from the error (90% confidence level) on the best-fit normalization. Solid lines show the model SEDs for the case $s = 2$.

GRB190114C: model

$s = 0, \varepsilon_e = 0.07, \varepsilon_B = 8 \times 10^{-5}, p = 2.6, n_0 = 0.5$ and $E_k = 8 \times 10^{53}$ erg

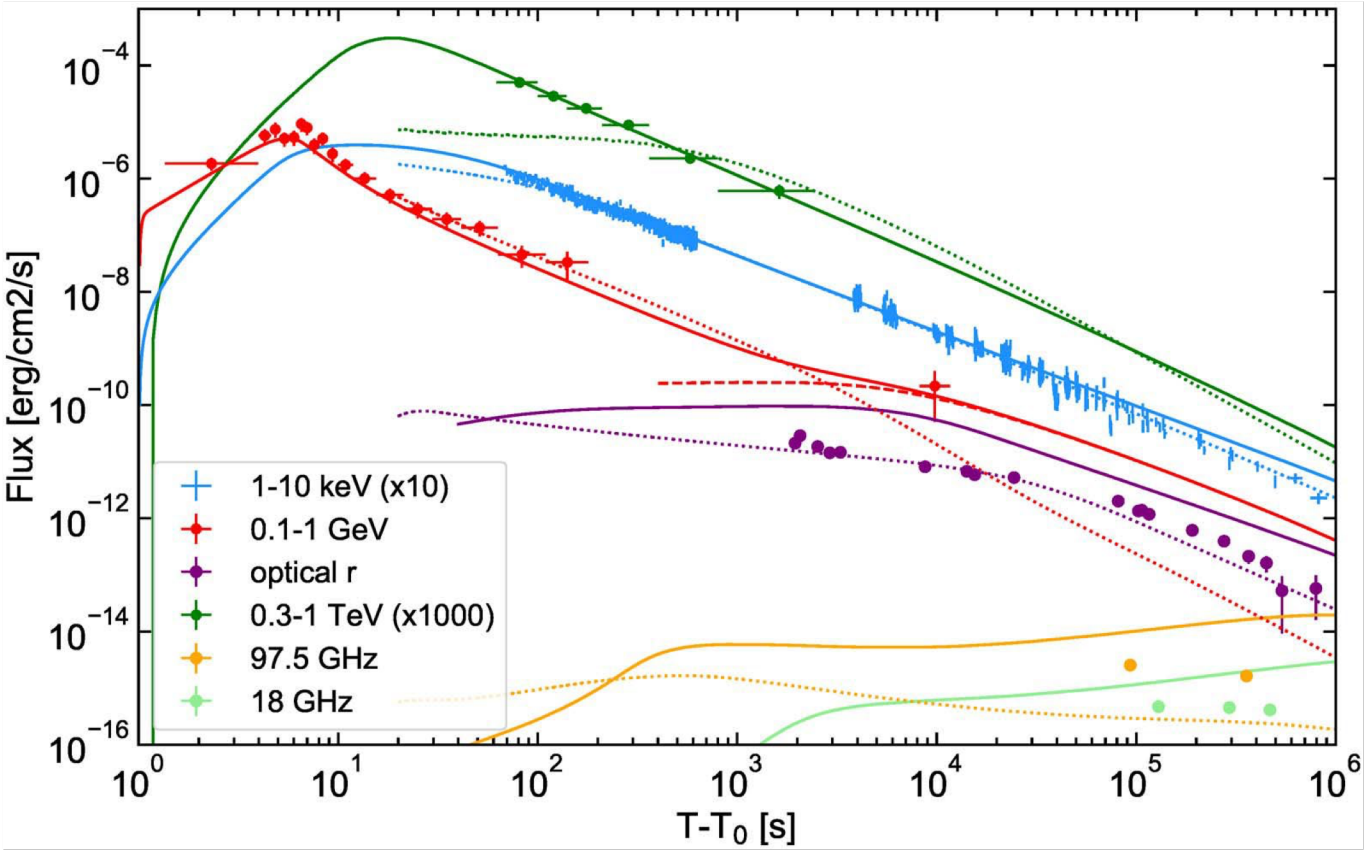

Extended Data Fig. 7 | Modelling of broadband light curves. Modelling results of forward shock emission are compared to observations at different frequencies (see key). The model shown with solid and dashed lines is optimized to describe the high-energy radiation (teraelectronvolt, gigaelectronvolt and X-ray) and has been obtained with the following parameters: $s = 0, \varepsilon_e = 0.07, \varepsilon_B = 8 \times 10^{-5}, p = 2.6, n_0 = 0.5$ and $E_k = 8 \times 10^{53}$ erg. Solid lines show the total flux (synchrotron and SSC) and the dashed line refers to the SSC contribution only. Dotted curves correspond to a better modelling of observations at lower frequencies, but fail to explain the behaviour of the teraelectronvolt light curve; they are obtained with the following model parameters: $s = 2, \varepsilon_e = 0.6, \varepsilon_B = 10^{-4}, p = 2.4, A_* = 0.1$ and $E_k = 4 \times 10^{53}$ erg. Vertical bars on the data points show the 1σ errors on the flux, and horizontal bars represent the duration of the observation.

Early NIR-V not modeled (RS) – Late radio: not reproduced.

Summary:

- Two nice and clear detections
- A new window on GRB afterglows
- Optimistic prospects for CTA

- Prompt TeV emission?

- Afterglow physics: is the external shock + SSC explanation enough?

  Things to investigate:
  effect of pair enrichment in external medium at early times,
  possible contribution of a long lived RS,
  …